# Ammonia Production via a Two-Step Al 2 O 3 /AlN Thermochemical Cycle. 2. Kinetic Analysis

**ARTICLE** *in* INDUSTRIAL & ENGINEERING CHEMISTRY RESEARCH · MARCH 2007

Impact Factor: 2.59 · DOI: 10.1021/ie061551m



**4 AUTHORS**, INCLUDING:

Maria Elena Galvez
Pierre and Marie Curie University - Paris 6
**66** PUBLICATIONS **828** CITATIONS

# Ammonia Production via a Two-Step $Al_2O_3$/AlN Thermochemical Cycle. 2. Kinetic Analysis

**M. E. Gálvez,[†] A. Frei,[‡] M. Halmann,[§] and A. Steinfeld*[,†,‡]**

*ETH Zurich, Department of Mechanical and Process Engineering, 8092 Zurich, Switzerland, Paul Scherrer Institute, Solar Technology Laboratory, 5232 Villigen PSI, Switzerland, and Department of Environmental Sciences and Energy Research, Weizmann Institute of Science, Rehovot 76100, Israel*

The production of ammonia via a two-step cyclic process is considered, consisting of an endothermic carbo-reduction of $Al_2O_3$ in a $N_2$ atmosphere to form AlN, followed by exothermic steam-hydrolysis of AlN to produce $NH_3$ and to reform $Al_2O_3$. The chemical kinetics of both steps were experimentally investigated by thermogravimetry and gas chromatography, without added catalysts and under external supply of process heat. Rate laws and the corresponding Arrhenius kinetic parameters were determined by applying the unreacted core model for the AlN production and the shrinking core model for the AlN hydrolysis.

## Introduction

In a previous paper,[1] we proposed and thermodynamically examined a novel cyclic process for the production of ammonia that involves two thermochemical steps. The first, high-temperature, endothermic step is the production of aluminum nitride by carbothermal reduction of alumina in a $N_2$ atmosphere. The second step is the hydrolysis of aluminum nitride to form ammonia and alumina; the latter is in turn recycled to the first step. The reaction steps can be represented by

$$\text{1st step: } Al_2O_3 + 3C + N_2 = 2AlN + 3CO \qquad \Delta H^0_{25°C} = 708.1 \text{ kJ mol}^{-1} \quad (1)$$

$$\text{2nd step: } 2AlN + 3H_2O = Al_2O_3 + 2NH_3 \qquad \Delta H^0_{25°C} = -274.1 \text{ kJ mol}^{-1} \quad (2)$$

CO produced in the first step may be further processed by the water−gas shift reaction to syngas and used as a fuel or as an intermediate to methanol or Fischer−Tropsch products. Relative to the conventional production of $NH_3$ via the Haber−Bosch process, the proposed two-step process offers the following 3-fold advantages: (1) it eliminates the need for high pressure, minimizing costs and safety concerns; (2) it eliminates the need for catalysts, minimizing costs associated with their production and recycling; and (3) it eliminates the need for hydrogen as feed stock, reducing energy consumption and $CO_2$ emissions. A preliminary environmental and economic analysis indicates favorable fuel economy and hence costs.[1] Furthermore, the use of concentrated solar energy as the source of high-temperature process heat for the endothermic carbothermic reduction reduces significantly or completely eliminates concomitant $CO_2$ emissions. Experimental studies on the carbothermal reduction of $Al_2O_3$ have been carried out at above 1500 °C in a high-flux solar furnace.[2,3]

Reaction 1 is highly endothermic ($\Delta H^0_{25°C} = 708.1$ kJ mol$^{-1}$) and thermodynamically favorable at above 1300 °C.[1] It has been carried out in electrical furnaces with reasonable rates at above 1400 °C.[4−6] One important current application is the large-scale production of high-quality AlN substrates with high thermal conductivity for the electronics industry.[5] Yields of up to 99% were reported at 1800 °C, using $Al_2O_3$ and carbon black in a stoichiometric ratio with a $N_2$ pressure of 0.3 MPa.[7] Tsuge and co-workers[8] found that $\gamma$-$Al_2O_3$ had the highest reactivity among the various forms of alumina. Chen et al.[9] observed that the reaction rate is enhanced by increasing the $N_2$ flow rate, temperature, and C/$Al_2O_3$ ratio and by decreasing particle size and initial bulk density. In contrast, Forslund and Zheng[4] showed that the conversion decreases with increasing $N_2$ flow rate. Chen and Lin[10] developed a mathematical model to predict the influence of the different reaction parameters. Lefort and Billy[5] suggested that the reaction mechanism comprises $Al_2O_3$ dissociation into Al (g) and $O_2$, followed by their reaction with $N_2$ and CO, respectively. Carbon serves to reduce the $O_2$ partial pressure to such an extent that $Al_2O_3$ dissociation and Al (g) nitration become effective. Forslund and Zheng[11] also suggested that the reaction proceeds in the gas phase between gaseous Al or $Al_2O$, $N_2$, and CO. Chen and Lin[12] proposed a mechanism that comprises a first stage solid-phase reaction between $Al_2O_3$ and C to form $Al_2O$ (g) and CO, followed by a second stage absorption of $Al_2O$ (g) on the surface of the solid grains where it finally reacts with CO and $N_2$ to form AlN. On the other hand, O'Donnell and Trigg[13] pointed to a solid−solid-type mechanism occurring at local sites on the precursor alumina grains and free carbon. The fact that no $Al_2O_3$-free AlN nuclei was observed in TEM images and NMR spectra, and that no weight loss in excess of the theoretical one was observed that would result from the evaporation of Al, along with the observation of crystallite growth from the outside toward the inside of the $Al_2O_3$ particle, supported a solid-state rather than a gaseous diffusion reaction mechanism.

Reaction 2 is exothermic ($\Delta H^0_{25°C} = -274.1$ kJ mol$^{-1}$) and thermodynamically favorable at temperatures below 375 °C; at above 375 °C, $Al_2O_3$, $N_2$, and $H_2$ are the stable products in equilibrium.[1] Li et al.[14] studied the stability of AlN in moist air with 80% relative humidity and postulated a three-stage process consisting of a slow hydrolysis to $Al_2O_3$/$Al(OH)_3$ controlled by solid surface properties, followed by a fast hydrolysis controlled by chemical reaction on the surface, and finally the formation of $Al(OH)_3$ around AlN controlled by mass transfer. Highfield and Bowen[15] and Krnel et al.[16] observed the degrada-

* Author to whom correspondence should be addressed. Fax: +41 44 6321065. E-mail: aldo.steinfeld@eth.ch.
[†] ETH Zurich.
[‡] Paul Scherrer Institute.
[§] Weizmann Institute of Science.

10.1021/ie061551m CCC: $37.00 
Published on Web 02/21/2007

tion of AlN powders suspended in water at ambient temperature, along with the formation of an $Al(OH)_3$ layer over the AlN surface.

In this paper, the chemical kinetics of both reaction steps, 1 and 2, are investigated experimentally by isothermal/dynamic thermogravimetry and gas chromatography under conditions of an external supply of process heat and without added catalysts. Appropriate rate laws were formulated, and the kinetic parameters were determined by fitting to the experimental results. The solid reactants and products are characterized in terms of particle size distributions, specific surface area, and porosity.

## Experimental Procedures

**$Al_2O_3$ Reduction.** The carbothermal reduction runs were carried out in a thermogravimeter system (TG, Netzsch STA 409). Samples of activated carbon (Fluka no. 05105) and α-$Al_2O_3$ (Fluka no. 06285) in a C/$Al_2O_3$ molar ratio of 6:1 were placed in a graphite crucible and in contact with a S-type thermocouple. The runs were performed in the temperature range of 1500−1700 °C. In the dynamic runs, samples were heated to 1700 °C at a rate of 20 K/min and under a $N_2$ reacting flow of 100 mL $min^{-1}$. (L means liters at normal conditions; mass flow rates are calculated at 273 K and 1 bar.) In the isothermal runs, samples were heated in Ar to the desired temperature at a rate of 20 K/min, and then kept isothermally under a $N_2$ reacting flow of 100 mL $min^{-1}$. The composition of the gaseous products was continuously monitored by gas chromatography (MTI Micro CG P200 GC, equipped with a MS5A column and a TC detector).

**AlN Hydrolysis.** The hydrolysis runs were carried out in a similar thermogravimeter (TG, Netzsch STA 409 CD) but equipped with a special electric furnace suitable for reactive atmospheres containing up to 100% steam at 1 bar total pressure. The reactive gas entered the furnace chamber from the bottom and flowed upward. Samples of pure AlN (Aldrich no. 24190−3) were placed in a 17 mm diameter $Al_2O_3$ crucible and in contact with a S-type thermocouple. The mass flow rates were adjusted by electronic flow controllers for Ar (Vögtlin Q-FLOW) and for water (Bronkhorst LIQUI-FLOW). The runs were performed in the temperature range of 900−1200 °C and using a $H_2O$−Ar reacting flow of 300 mL $min^{-1}$ with steam concentrations of 20, 40, 60, and 80%. In the dynamic runs, samples were heated from 150 to 1200 °C at a rate of 10 K $min^{-1}$. In the isothermal runs, samples were heated in Ar to the desired reaction temperature at a rate of 10 K $min^{-1}$ and then kept isothermally under a $H_2O$−Ar reacting flow. The composition of the gaseous products was continuously monitored by gas chromatography (two-channel Varian Micro GC, equipped with Molsieve-5A and Poraplot-U columns). The gas exiting the thermogravimeter was flown through an impinger containing 35 mL of 0.1 M HCl. The amount of ammonia was measured by back-titration of the excess of HCl with 0.1 M NaOH, using phenolphthalein as an indicator.

The extent of the $Al_2O_3$ reduction, reaction (1), and of the AlN hydrolysis, reaction (2), is defined as

$$X_{\text{reaction(1)}} = 1 - \frac{n_{Al_2O_3}{}^{t}}{n_{Al_2O_3}{}^{0}} \tag{3}$$

$$X_{\text{reaction(2)}} = 1 - \frac{n_{AlN_3}{}^{t}}{n_{AlN}{}^{0}} \tag{4}$$

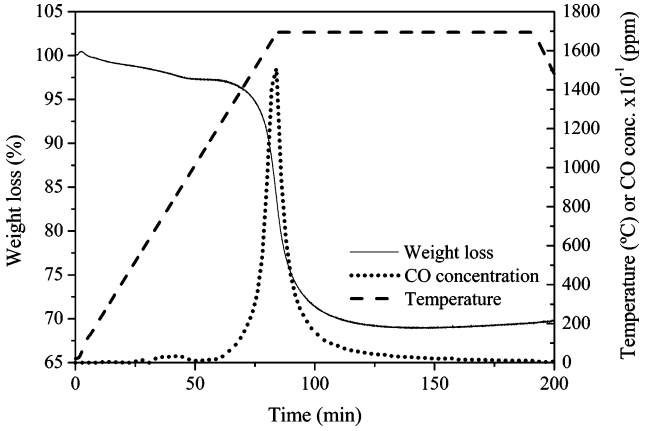


**Figure 1.** Relative weight loss (percent), temperature (°C), and CO concentration (ppm) in the outlet gas as a function of time during the TG-dynamic run of the carbothermal reduction of $Al_2O_3$ in $N_2$.

respectively, where $n_{Al_2O_3}{}^{t}$ and $n_{AlN}{}^{t}$ are the number of moles at a time $t$ of reaction, and $n_{Al_2O_3}{}^{0}$ and $n_{AlN}{}^{0}$ are the initial number of moles of $Al_2O_3$ and AlN, respectively. The ammonia yield in the AlN hydrolysis is defined as the number of $NH_3$ moles in the gas products relative to $n_{AlN}{}^{0}$.

Before and after the $Al_2O_3$ reduction and the AlN hydrolysis, the samples were characterized by means of particle size distributions (HORIBA LA-950 analyzer), $N_2$ adsorption (Micromeritics 3000), and X-ray powder diffraction (XRD, Phillips XPert-MPD powder difractometer). For the $N_2$ adsorption analysis, samples were degasified at 200 °C during 2 h prior to obtaining adsorption isotherms at −196 °C. The BET equation was applied for the calculation of specific surface area. Total micropore, narrow micropore, wide micropore, and mesopore volumes were determined by the *t*-plot empirical method.[17]

## Results and Discussion

**$Al_2O_3$ Reduction.** Figure 1 shows the relative weight loss, temperature, and CO concentration in the outlet gas as a function of time during the TG-dynamic run of the carbothermal reduction of $Al_2O_3$ in $N_2$. A 5% weight loss took place up to 1400 °C, attributed to the devolatilization of activated carbon. It followed a sharp decrease in the sample weight of about 30% of its initial weight and reached a maximum slope at 1700 °C. The CO peak corresponds to the sharp weight loss detected in the 1400−1700 °C range, corroborating the transformation according to reaction 1.

The reaction extent $X_{\text{reaction(1)}}$ as a function of time, obtained during the TG-isothermal runs of the carbothermal reduction of $Al_2O_3$ in $N_2$, reaction 1, is shown in Figure 2a,b. The parameter is the reaction temperature in the range of 1500−1700 °C, every 50 °C. In these figures, the markers correspond to the experimental data, and the solid lines correspond to the reaction extent obtained from two different kinetic models presented in the next section. Increasing the reaction temperature leads to a noticeable rate and yield increase. For example, a 3-fold increase in the $Al_2O_3$ conversion after 200 min is observed between 1550 and 1600 °C, with yields of 40 and 80%, respectively. The higher conversion of $Al_2O_3$ ($X_{\text{reaction(1)}}$ = 83%) was obtained after 30 min at 1700 °C, with a relative weight loss of 32%, which closely matches the theoretical one of 34%. This fact supports a solid−solid reaction mechanism with solid diffusion as the rate-limiting step[13] since if Al (g) and $Al_2O$ (g) were to be formed as suggested for a gas-phase mechanism,[5,11] a higher relative weight loss is to be expected along with Al condensation downstream, both of which were

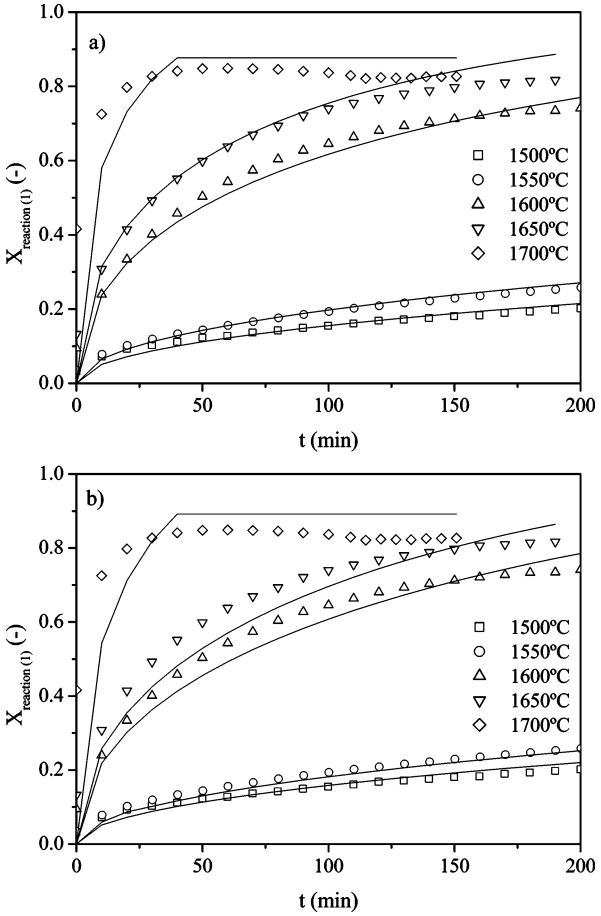


**Figure 2.** Extent of the carbothermal reduction of $Al_2O_3$ in $N_2$ as a function of time, obtained by TG-isothermal runs. The parameter is the reaction temperature in the range of 1500−1700 °C, every 50 °C. Markers correspond to the experimental data; solid lines correspond to kinetic modeling using (a) Jander's rate law and (b) Ginstling−Brounshtein's rate law.

not observed. Furthermore, the presence of a gaseous species such as $Al_2O$ (g) or Al (g) is thermodynamically unfavorable until up to 1984 and 4322 °C, respectively.[1]

The unreacted core model is applied to derive the Jander and the Ginstling−Brounshtein rate laws,[18] given by eqs 5 and 6, respectively

$$\frac{dX_{\text{reaction}(1)}}{dt} = k_{\text{Jander}} \frac{[3(1 - X_{\text{reaction}(1)})^{2/3}]}{[2(1 - (1 - X_{\text{reaction}(1)})^{1/3})]} \quad (5)$$

$$\frac{dX_{\text{reaction}(1)}}{dt} = k_{\text{Ginstling-Brounshtein}} \frac{3}{[2((1 - X_{\text{reaction}(1)})^{-1/3} - 1)]} \quad (6)$$

or in their integrated form

$$[1 - (1 - X_{\text{reaction}(1)})^{1/3}]^2 = k_{\text{Jander}} t \quad (7)$$

$$1 - \frac{2X_{\text{reaction}(1)}}{3} - (1 - X_{\text{reaction}(1)})^{2/3} = k_{\text{Ginstling-Brounshtein}} t \quad (8)$$

The temperature dependence of $k$ is determined by imposing an Arrhenius rate law, $k = k_0 e^{-E_a/RT}$. Arrhenius plots of the TG-isothermal data obtained for the carbothermal reduction of $Al_2O_3$ in $N_2$ are shown in Figure 3, by applying (a) Jander's rate law and (b) Ginstling−Brounshtein's rate law. The kinetic parameters $k_0$ and $E_a$, determined by linear regression, are listed in

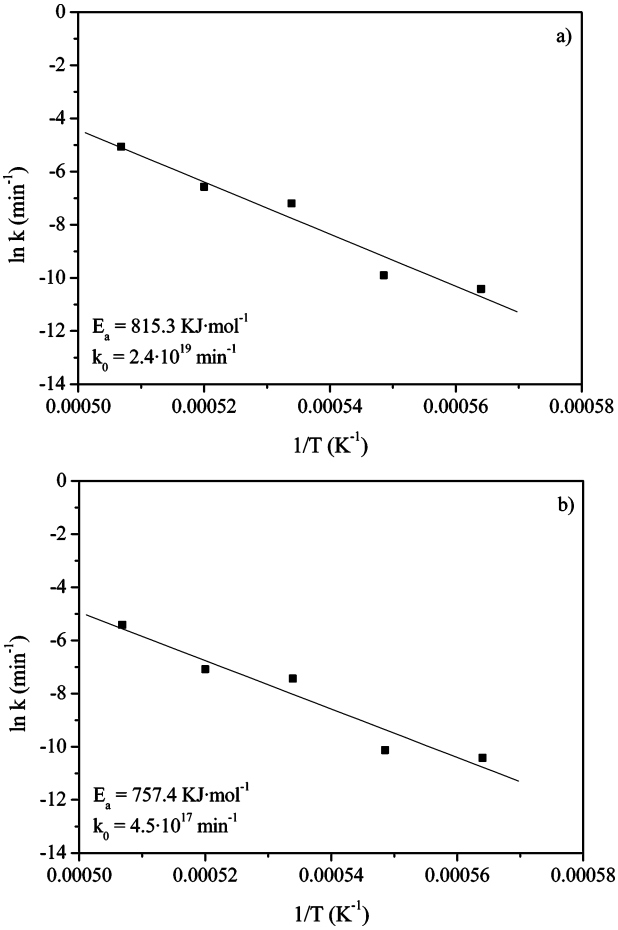


**Figure 3.** Arrhenius plots of the TG-isothermal data obtained for the carbothermal reduction of $Al_2O_3$ in $N_2$, by applying: (a) Jander's rate law and (b) Ginstling−Brounshtein's rate law.

**Table 1. Arrhenius Kinetic Parameters for the Carbothermal Reduction of $Al_2O_3$ in $N_2$**

| rate law | $E_a$ (kJ mol$^{-1}$) | $k_0$ (min$^{-1}$) | rms | $R^2$ |
|---|---|---|---|---|
| Jander | 815.3 | $2.4 \times 10^{19}$ | 0.053 | 0.9544 |
| Ginstling−Brounshtein | 757.4 | $4.5 \times 10^{17}$ | 0.06 | 0.9346 |

Table 1 for both rate laws. The values for $E_a$ are higher than those reported by Lefort et al.[5] (384 kJ mol$^{-1}$), who applied the classical unreacted core model with gas−solid surface chemical reaction control. As expected, a solid-state reaction with solid diffusion control is energetically more demanding. The solid lines in Figure 2a,b correspond to the predicted reaction extent calculated using Jander's and Ginstling-Brounshtein's rate law, respectively. The accuracy of the fitting is determined by the $R^2$ value and the rms error, defined as

$$R^2 = 1 - \left[ \frac{\sum_{i=1}^{n} (Y_i - \bar{Y}_i)^2}{\sum_{i=1}^{n} Y_i^2 - \frac{(\sum_{i=1}^{n} Y_i)^2}{n}} \right]; \quad \text{rms} = \sqrt{\frac{\sum_{i=1}^{n} (Y_i - \bar{Y}_i)^2}{n}} \quad (9)$$

where Yi and $\bar{Y}_i$ are the experimental and calculated values, respectively, and $n$ is the number of data. $R^2$ and rms values are listed in Table 1. A slightly better fitting to the experimental data is obtained with Jander's model, which has been applied in previous studies.[19,20]

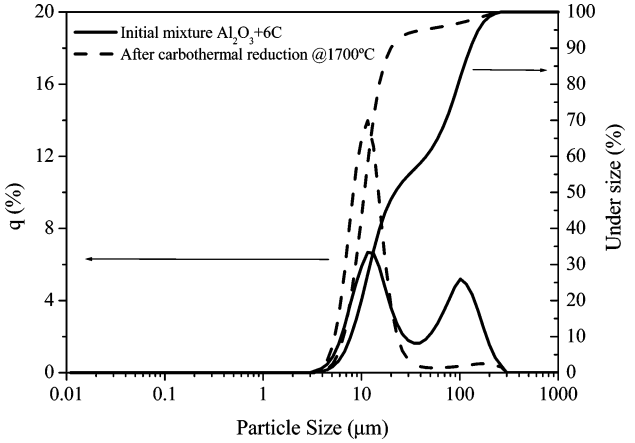


**Figure 4.** Particle size distributions of the solids before and after the carbothermal reduction of $Al_2O_3$ in $N_2$.

As it will be shown in the particle analysis that follows, activated carbon is characterized by a porous structure and a large specific surface area. It further contains impregnation agents that, upon pyrolysis, release CO, $H_2$, and other reducing gases, which in turn start the chain process of gas-phase reduction of $Al_2O_3$, influencing its kinetics. However, these pyrolytic gases generated at below 1400 °C are swept out of the reaction chamber by the carrier gas (Ar or $N_2$) before the carboreduction temperature is attained. Nevertheless, the morphology of the reducing agent may affect the reaction rate. Comparative runs were carried out with petroleum coke and beech charcoal as reducing agents, resulting in higher reaction rates and apparent activation energies of 636.6 and 454.5 kJ/mol, respectively, by applying Jander's model with fittings $R^2 = 0.99$ and 0.92, respectively.

The amount of CO measured by GC was compared with the one calculated by mass balance using the TG data. Accounted as well was the CO derived by pyrolysis of activated carbon, determined in separate runs without $Al_2O_3$. The agreement is within 20%. The main source of measurement error is due to the mass flow rate controller.

Figure 4 shows the results of the particle size analysis for the initial solid reactants and for the solid products after carbothermal reduction at 1700 °C. The initial mixture has a bimodal size distribution with particles of mean sizes of 12 and 100 $\mu$m, corresponding to C and $Al_2O_3$, respectively. After carbothermal reduction, the $Al_2O_3$ grains underwent transformation to AlN, and the particle size distribution of the products has only a small shoulder after a sharp peak centered in 12−15 $\mu$m.

Table 2 shows the results of the textural characterization of solid reactants and products of the carbothermal reduction of $Al_2O_3$ in $N_2$. The initial $Al_2O_3$ is clearly a nonporous solid, while the activated carbon has a wider distribution of pore sizes, offering a larger specific surface area. As expected, the $Al_2O_3$ + 6C mixture shows an intermediate $S_{BET}$ value and exhibits both micropores and mesopores. The analysis of the products

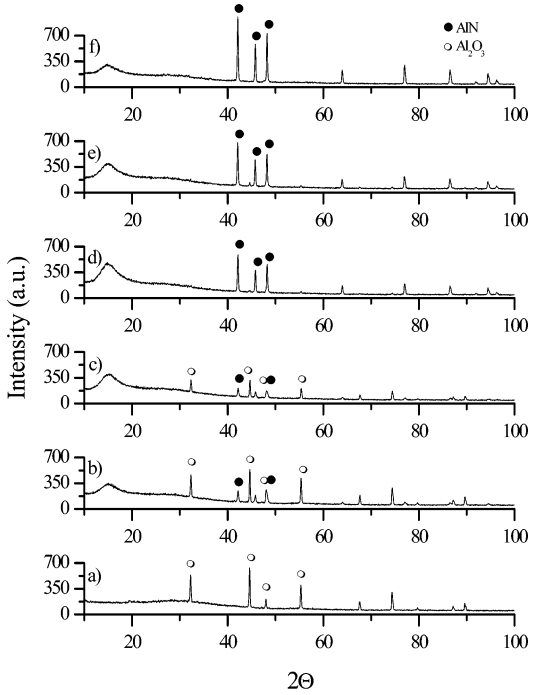


**Figure 5.** XRD patterns for the (a) $Al_2O_3$ + 6C reacting mixture and for the solid products after carbothermal reduction at (b) 1500 °C, (c) 1550 °C, (d) 1600 °C, (e) 1650 °C, and (f) 1700 °C.

reveals a 2-fold decrease in the specific surface area and a considerable decrease in the micropore and mesopore volume. Furthermore, $S_{BET}$ decreased with the reaction temperature. During the heating phase to 1500−1700 °C, activated carbon contained in the reactant mixture lost volatile matter and underwent a reorganization of the graphitic planar layers, giving rise to a less porous structure. Presumably, this graphitized material along with the formation of AlN crystals accounts for the mesoporosity observed in the carbothermal reduction products. When complete conversion was attained, the solids products were practically free of micropores. The XRD patterns for the initial $Al_2O_3$ + 6C reacting mixture and for the solid products obtained after carbothermal reduction at 1500, 1550, 1600, 1650, and 1700 °C are shown in Figure 5. The reflections corresponding to $Al_2O_3$ decrease in intensity as the reaction temperature increases and disappear at above 1600 °C. Interestingly, a first broad reflection at low $2\theta$ is observed in the products at all temperatures but not in the pattern for the reacting mixture. This band is attributed to graphitized carbon material obtained by thermal treatment during the heating phase.

A semiquantitative estimation of the extent of reaction 1 was performed by integrating the area below the peaks of the more intense XRD reflections corresponding to pure $Al_2O_3$ ($2\theta$ = 44.6 and 55.3°) and to pure AlN ($2\theta$ = 42.1 and 45.8°) and by relating the ratio between these areas to the ones observed with calibrated samples. Figure 6 shows the calibration line: a second order polynomial for the calculation of AlN concentration as a

**Table 2. Textural Characterization of Solid Reactants and Products of the Carbothermal Reduction of $Al_2O_3$ in $N_2$**

| | sample | $S_{BET}$ ($m^2\ g^{-1}$) | $V_{microporetotal}$ ($cm^3\ g^{-1}$) | $V_{micropore<0.7nm}$ ($cm^3\ g^{-1}$) | $V_{micropore\_medium\_size}$ ($cm^3\ g^{-1}$) | $V_{mesopore}$ ($cm^3\ g^{-1}$) |
|---|---|---|---|---|---|---|
| reactants | $Al_2O_3$ | 3.4 | 0 | 0 | 0 | 0.0042 |
| | activated carbon | 1066.2 | 0.4263 | 0.1446 | 0.2818 | 0.1832 |
| | $Al_2O_3$ + 6C | 408.5 | 0.1534 | 0.0735 | 0.0799 | 0.0855 |
| products | @ 1500 °C | 242.2 | 0.0644 | 0.0126 | 0.0264 | 0.0519 |
| | @ 1600 °C | 163.9 | 0.0044 | 0 | 0.0044 | 0.2831 |
| | @ 1700 °C | 163.1 | 0.0175 | 0 | 0.0175 | 0.1937 |
| AlN Aldrich no. 24190-3 | | 6.7 | 0 | 0 | 0 | 0.0104 |

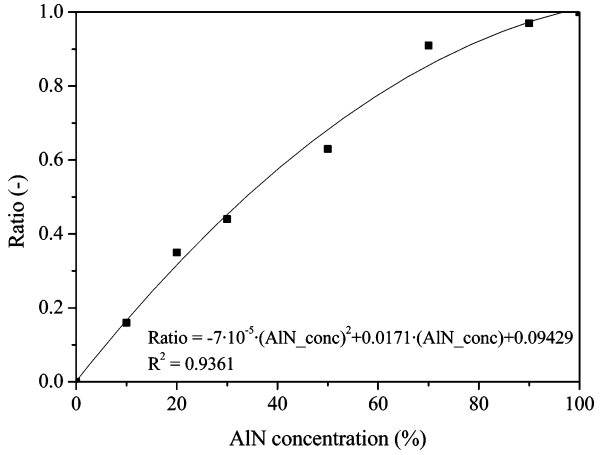


**Figure 6.** Ratio between the areas of the XRD patterns corresponding to the most important XRD reflections of pure $Al_2O_3$ ($2\theta$ = 44.6 and 55.3°) and of pure AlN ($2\theta$ = 42.1 and 45.8°) as a function of the AlN concentration in AlN−$Al_2O_3$ mixtures.

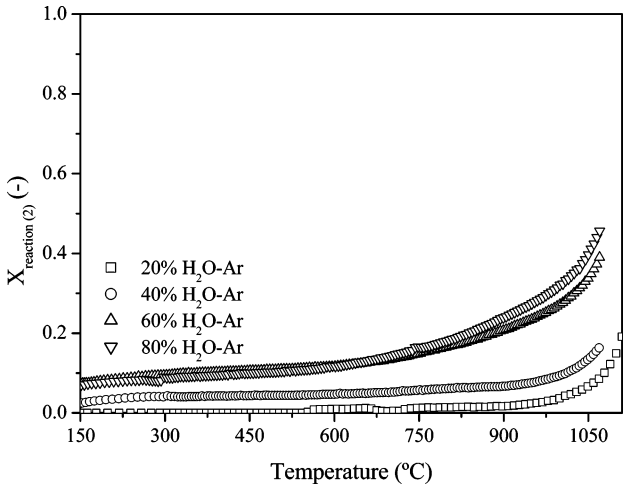


**Figure 7.** Extent of the AlN hydrolysis as a function of temperature, obtained by TG-dynamic runs with 20, 40, 60, and 80% steam concentrations in the $H_2O$−Ar reacting gas. The heating rate is 10 K/min.

**Table 3. Extent of the Carbothermal Reduction of $Al_2O_3$ in $N_2$ after 200 Min as a Function of the Reaction Temperature, Determined by TG and XRD**

| reaction temperature (°C) | $X_{reaction(1)}$ from TG | $X_{reaction(1)}$ from XRD |
|---|---|---|
| 1500 | 0.20 | 0.16 |
| 1550 | 0.26 | 0.27 |
| 1600 | 0.74 | 0.87 |
| 1650 | 0.82 | 0.83 |
| 1700 | 0.83 | 0.93 |

function of the ratio between the areas of the XRD patterns in different mixtures of AlN (Aldrich no. 24190−3) and $Al_2O_3$ (Fluka no. 06285). The $R^2$ of the regression is 0.9361. Table 3 lists the extent of the carbothermal reduction of $Al_2O_3$ in $N_2$ after 200 min as a function of temperature, determined by both TG and XRD. The differences are attributed to the inaccuracies associated with surface and punctual XRD measurements, but generally, reasonable agreement is obtained between the two experimental data sources.

**AlN Hydrolysis.** The reaction extent of the AlN hydrolysis, $X_{reaction(2)}$, as a function of temperature obtained by TG-dynamic runs, is shown in Figure 7 for various steam concentrations in the $H_2O$−Ar reacting gas. The reaction proceeds already at low temperatures, but its rate is notably accelerated at above 900 °C. The reaction rate and, consequently, the reaction extent increase with the steam concentration in the reaction gas. For example, at 1000 °C, the reaction extent reaches 27 and 32%, with 40 and 60% $H_2O$−Ar, respectively.

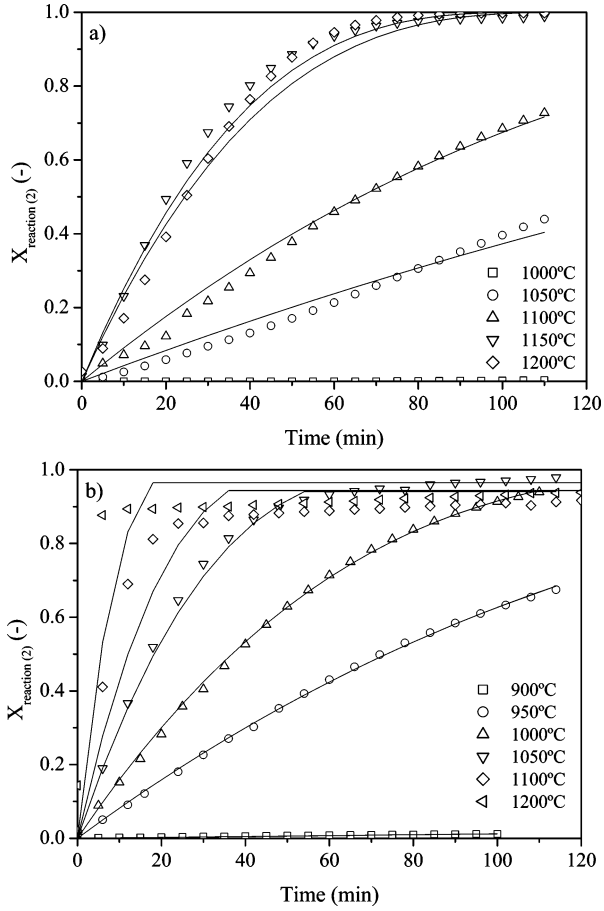


**Figure 8.** Extent of the AlN hydrolysis as a function of time, obtained by TG-isothermal runs at temperatures from 900 to 1200 °C with (a) 10% $H_2O$−Ar and (b) 80% $H_2O$−Ar. Markers correspond to experimental data; solid lines correspond to the kinetic modeling based on a shrinking core with surface chemical reaction control.

The reaction extent of the AlN hydrolysis, $X_{reaction(2)}$, a function of time obtained by TG-isothermal runs at 900, 1000, 1050, and 1200 °C is shown in Figure 8 using (a) 10% $H_2O$−Ar and (b) 80% $H_2O$−Ar. In this figure, the markers correspond to the experimental data, and the solid lines correspond to the kinetic model described in the following section. The reaction proceeds notably faster with higher steam concentration, supporting a surface chemical reaction rate-controlling mechanism.[21] For example, for reaching an AlN conversion of 90% at 1200 °C, the reaction time requirement is 50 and 5 min for 10 and 80% $H_2O$−Ar, respectively. No significant reaction occurs at below 900 and 1050 °C with 80 and 10% $H_2O$−Ar, respectively.

The shrinking core model was applied.[21] Assuming surface chemical reaction rate-controlling mechanisms for spherical particles, the rate law is given by

$$1 - (1 - X_{reaction(2)})^{1/3} = kt \qquad (10)$$

where $k$ is a function of the intrinsic kinetic constant, solid density, initial particle diameter, and the water vapor partial pressure. Figure 8a,b shows the reaction extents as a function of time as predicted by this model. The rms values of the difference between the model calculated and the experimentally obtained curves are 0.032 and 0.05 for 10% $H_2O$−Ar and 80% $H_2O$−Ar, respectively. Figure 9 shows the Arrhenius plots for $k$, eq 10. The values have been normalized to account for the

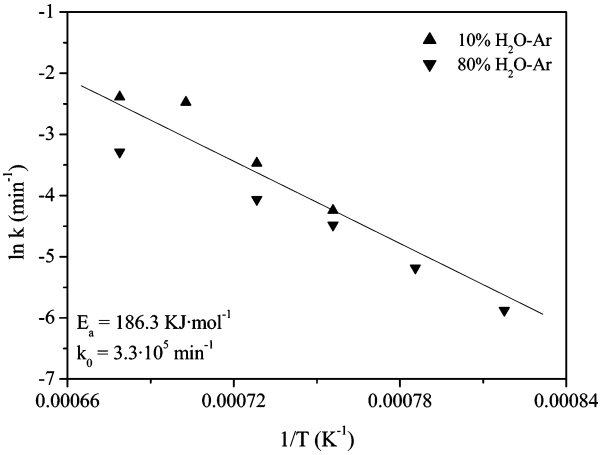


**Figure 9.** Arrhenius plot for the TG-isothermal data obtained for the AlN-hydrolysis with 10% $H_2O$−Ar and 80% $H_2O$−Ar, by applying the shrinking core model.

**Table 4. Reaction Extent (Measured by TG) and Ammonia Yield (Determined by Mass Balance on $H_2$, Measured by GC) for the Hydrolysis of AlN Using 80% $H_2O$−Ar Mixture at Different Temperatures**

| reaction temperature (°C) | $X_{reaction(2)}$ | $NH_3$ yield (%) |
|---|---|---|
| 950 | 0.68 | 65 |
| 1000 | 0.93 | 88 |
| 1100 | 0.95 | 81 |
| 1200 | 0.94 | 74 |

water vapor concentration employed in each set of experiments. Indicated also are the apparent activation energy and frequency factors, obtained by linear regression.

According to thermodynamic computations on the 2AlN + $3H_2O$ system, $H_2$ and $N_2$ are stable gaseous products in equilibrium at above 375 °C and 1 bar;[1] however, the presence of metastable $NH_3$ is possible in the absence of catalysts. The ammonia content was determined by mass balance on $H_2$ measured by GC, assuming complete condensation of excess water from the gaseous products. Main error sources are the uncertainty on the total mass flow rate of gaseous products (due to partial condensation of water vapor) and the possible oxidation of $H_2$ to form additional $H_2O$. Table 4 shows the reaction extent and ammonia yield obtained for the hydrolysis of AlN using the 80% $H_2O$−Ar mixture at different temperatures. A maximum $NH_3$ yield of 88% was obtained at 1000 °C for a 93% reaction extent. At higher temperatures the yield decreased, presumably as a result of the thermodynamically favorable dissociation of $NH_3$. The $NH_3$ yield was also measured by back-titration of HCl. The main error source in this methodology is the uncompleted retention of $NH_3$ by HCl. The value measured at 1200 °C was comparable to the one determined by mass balance on $H_2$.

Figure 10 shows the results of the particle size analysis of AlN and the product of its hydrolysis in the presence of 80% $H_2O$−Ar at 1200 °C. Raw AlN has a bimodal distribution of particle sizes with two mean sizes of 0.09 and 5 $\mu$m, respectively. After hydrolysis, the particle size increases, yielding a material with a mean size of 10 $\mu$m, presumably due to the growing of an $Al_2O_3$ layer over the AlN core.

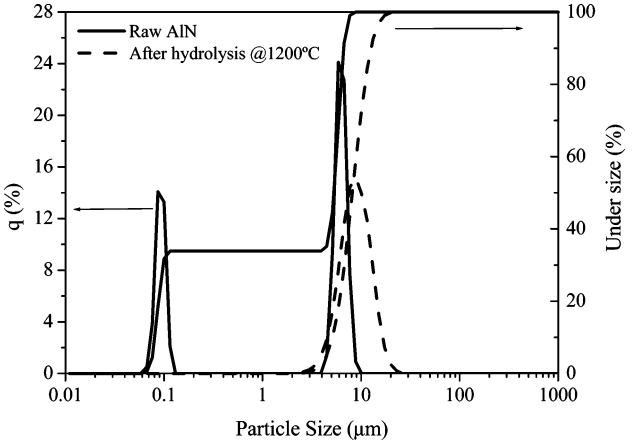


**Figure 10.** Particle size analysis of the solids before and after the hydrolysis of AlN.

Table 5 shows the textural characterization of solid reactants and products of the hydrolysis of AlN with 80% $H_2O$−Ar. Porosity slightly increases after hydrolysis. Solid products exhibited only a small amount of mesopores and practically no microporosity, similar to the characteristics of commercial $Al_2O_3$ (Fluka no. 06285) employed for the carbothermal reduction. The XRD patterns of the initial AlN and of the solid products obtained after hydrolysis with 80% $H_2O$−Ar at 900, 1000, 1050, and 1200 °C are shown in Figure 11. The reflections corresponding to AlN decrease in intensity as the reaction temperature increases and disappear at above 1000 °C, in agreement with the TG results. In analogy to the carbothermal reduction, a semiquantitative estimation of the extent of reaction 2 was performed using the calibration curve of Figure 6. Table 6 lists the extent of the hydrolysis of AlN with 80% $H_2O$−Ar after 120 min as a function of temperature, determined by both TG and XRD. Except for the values obtained at the lower reaction temperature, good agreement is obtained between the two experimental data sources.

## Conclusion

We have performed a thermogravimetric kinetic analysis of the two reactions involved in the two-step cyclic process for $NH_3$ production. The carbothermal reduction of $Al_2O_3$ with activated carbon was investigated in the 1500−1700 °C range. Its reaction extent exceeded 80% at 1700 °C after 30 min. The solid−solid diffusion models of Jander and of Ginstling−Brounshtein were applied with reasonable agreement, yielding activation energies of 815 and 757 kJ $mol^{-1}$, respectively. XRD and $N_2$ adsorption characterization of the reactants and solid products revealed a significant decrease of the porosity after the reaction and with increasing reaction temperature. The hydrolysis of AlN was investigated in the 900−1200 °C range with steam concentrations of 20, 40, 60, and 80%. The reaction

**Table 5. Textural Characterization of the Solid Reactants and Products of the Hydrolysis of AlN with 80% $H_2O$−Ar**

| | sample | $S_{BET}$ ($m^2$ $g^{-1}$) | $V_{microporetotal}$ ($cm^3$ $g^{-1}$) | $V_{micropore<0.7nm}$ ($cm^3$ $g^{-1}$) | $V_{micropore\_medium\_size}$ ($cm^3$ $g^{-1}$) | $V_{mesopore}$ ($cm^3$ $g^{-1}$) |
|---|---|---|---|---|---|---|
| reactants | AlN | 6.7 | 0 | 0 | 0 | 0.0104 |
| products | @ 900 °C | 13.1 | 0 | 0 | 0 | 0.0194 |
| | @ 1000 °C | 11.3 | 0 | 0 | 0 | 0.0121 |
| | @ 1050 °C | 11.2 | 0 | 0 | 0 | 0.0118 |
| | @ 1200 °C | 12.1 | 0 | 0 | 0 | 0.0121 |
| $Al_2O_3$ Fluka no. 06285 | | 3.4 | 0 | 0 | 0 | 0.0042 |

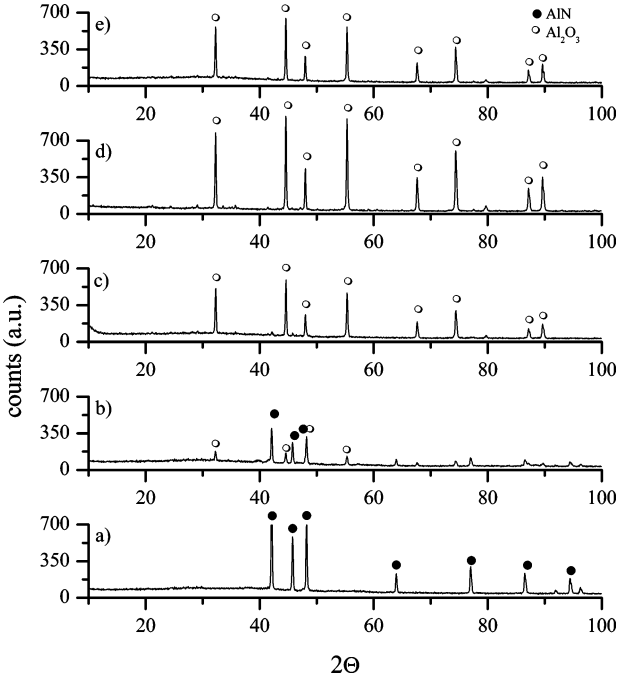


**Figure 11.** XRD patterns of (a) the initial AlN and of the solid products obtained after hydrolysis with 80% $H_2O$−Ar at (b) 900 °C, (c) 1000 °C, (d) 1050 °C, and (e) 1200 °C.

**Table 6. Extent of the Hydrolysis of AlN with 80% $H_2O$−Ar after 120 Min as a Function of the Reaction Temperature, Determined by TG and XRD**

| reaction temperature (°C) | $X_{reaction2}$ from TG | $X_{reaction2}$ from XRD |
|---|---|---|
| 900 | 0.01 | 0.46 |
| 1000 | 0.93 | 0.96 |
| 1050 | 0.98 | 0.99 |
| 1200 | 0.94 | 1 |

proceeded at reasonable rates above 900 °C, reaching completion (from AlN to $Al_2O_3$) after 120 min with 80% $H_2O$−Ar. The yield of $NH_3$, determined by back-titration, was diminished because of its thermodynamically favorable dissociation at high temperatures. The classical shrinking core model adequately described the experimental data, yielding an apparent activation energy of 186.3 kJ $mol^{-1}$. Maximum yield of ammonia was obtained at a temperature of 1000 °C. The reaction extents obtained by TG analysis were verified using calibrated XRD patterns for both reaction steps.

## Acknowledgment

We thank D. Wuethrich for his help in performing the thermogravimetric runs.

## Nomenclature

$E_a$ = activation energy (kJ $mol^{-1}$)
$K$ = kinetic rate constant ($min^{-1}$)
$k_0$ = Arrhenius frequency factor ($min^{-1}$)
$n_{Al_2O_3}^0$ = initial number of moles of $Al_2O_3$ (mol)
$n_{AlN}^0$ = initial number of moles of AlN (mol)
$n_{Al_2O_3}^t$ = number of moles of $Al_2O_3$ at time $t$ (mol)
$n_{AlN}^t$ = number of moles of AlN at time $t$ (mol)
$R^2$ = $R$-squared value
rms = rms error
$S_{BET}$ = BET surface area ($m^2$ $g^{-1}$)
$T$ = temperature (K)
$t$ = time (min)
$X_{reaction(1)}$ = extent of reaction 1
$X_{reaction(2)}$ = extent of reaction 2
XRD = X-ray powder diffraction
$\Delta H_r^0{}_{25°C}$ = standrad enthalpy change of reaction at 25 °C (kJ $mol^{-1}$)

## Literature Cited

(1) Gálvez, M. E.; Halmann, M.; Steinfeld, A. Ammonia production via a two-step $Al_2O_3$/AlN thermochemical cycle. 1. Thermodynamic, environmental, and economic analyses. *Ind. Eng. Chem. Res.* **2007**, *46*, 2042−2046.

(2) Murray, J. P.; Steinfeld, A.; Fletcher, E. Metals, nitrides, and carbides via solar carbothermal reduction of metal oxides. *Energy* **1995**, *20*, 695−704.

(3) Murray, J. P. Solar production of aluminum by direct reduction of ore to Al−Si alloy: Preliminary results for two processes. *J. Solar Energy Eng.* **2001**, *123*, 125−132.

(4) Forslund, B.; Zheng, J. Carbothermal synthesis of aluminum nitride at elevated nitrogen pressures. Part I. Effect of process parameters on conversion rate. *J. Mater. Sci.* **1993**, *28*, 3125−3131.

(5) Lefort, P.; Billy, M. Mechanism of AlN formation through the carbothermal reduction of $Al_2O_3$ in a flowing $N_2$ atmosphere. *J. Am. Ceram. Soc.* **1993**, *76*, 2295−2299.

(6) Stroup, P. T. Carbothermic smelting of aluminum. *Trans. Metall. Soc. AIME* **1964**, *230*, 356−372.

(7) Makarenko, G. N. Features of carbothermic synthesis of aluminum nitride under nitrogen pressure. *Powder Metall. Met. Ceram.* **2002**, *41*, 232−236.

(8) Tsuge, A.; Inoue, H.; Kasori, M.; Shinozaki, K. Raw material effect on AlN powder synthesis from $Al_2O_3$ carbothermal reduction. *J. Mater. Sci.* **1990**, *25*, 2359−2361.

(9) Chen, H.-K.; Lin, C.-I.; Lee, C. Kinetics of the reduction of carbon/alumina powder mixture in a flowing nitrogen stream. *J. Am. Ceram. Soc.* **1994**, *77*, 1753−1756.

(10) Chen, H.-K.; Lin, C.-I. A mathematical model of carbothermic nitridation of carbon/alumina powder mixture. *J. Chem. Eng. Jpn.* **1994**, *27*, 90−94.

(11) Forslund, B.; Zheng, J. Carbothermal synthesis of aluminum nitride at elevated nitrogen pressures. Part II. Effect of process parameters on particle size and morphology. *J. Mater. Sci.* **1993**, *28*, 3132−3136.

(12) Chen, H.-K.; Lee, C.-I. Mechanism of the reduction of carbon/alumina powder mixture in a flowing nitrogen stream. *J. Mater. Sci.* **1994**, *29*, 1352−1357.

(13) O'Donnell, R. G.; Trigg, M. B. The mechanism of conversion of $Al_2O_3$ to AlN via carbothermal synthesis. *Micron* **1994**, *25*, 575−579.

(14) Li, J.; Nakamura, M.; Shirai, T.; Matsumaru, K.; Ishizaki, C.; Ishizaki, K. Mechanism and kinetics of aluminium nitride powder degradation in moist air. *J. Am. Ceram. Soc.* **2006**, *89*, 937−943.

(15) Highfield, J. G.; Bowen, P. Diffuse-reflectance Fourier transform infrared spectroscopic studies of the stability of aluminum nitride powder in an aqueous environment. *Anal. Chem.* **1989**, *61*, 2399−2402.

(16) Krnel, K.; Dra_iè, G.; Kosmaè, T. Degradation of AlN powder in aqueous environments. *J. Mater. Res.* **2004**, *19*, 1157−1163.

(17) Gregg, S. J.; Sing, K. S. W. *The physical adsorption of gases by non-porous solids: The type II isotherm, adsorption, surface area, and porosity*; Academic Press: London, 1982; pp 41−105.

(18) Shimizu, A.; Hao, Y.-J. Influence of particle contact on the estimation of powder reaction kinetics of binary mixtures. *J. Am. Ceram. Soc.* **1997**, *80*, 557−568.

(19) Babushkin, O.; Lindbäck, T.; Luc, J.-C.; Leblais, J.-Y. M. Kinetic aspects of the formation of lead zirconium titanate. *J. Eur. Ceram. Soc.* **1996**, *16*, 1293−1298.

(20) Paik, J.-G.; Lee, M.-J.; Hyun, S.-H. Reaction kinetics and formation mechanism of magnesium ferrites. *Thermochim. Acta* **2005**, *425*, 131−136.

(21) Levenspiel, O. *Chemical reaction engineering*, 3rd ed.: John Wiley and Sons: New York, 1999.

*Received for review* December 3, 2006
*Revised manuscript received* January 8, 2007
*Accepted* January 18, 2007

IE061551M